



1 **Environmental signal shredding on sandy coastlines**

2 Eli D. Lazarus<sup>1\*</sup>, Mitchell D. Harley<sup>2</sup>, Chris E. Blenkinsopp<sup>3</sup> and Ian L. Turner<sup>2</sup>

3 <sup>1</sup>Environmental Dynamics Lab, School of Geography and Environment, University of  
4 Southampton, Southampton, UK

5 <sup>2</sup>Water Research Laboratory, School of Civil and Environmental Engineering, University of  
6 New South Wales, Sydney NSW, Australia

7 <sup>3</sup>Research Unit for Water, Environment and Infrastructure Resilience (WEIR), University  
8 of Bath, Bath, UK

9 \*correspondence to: [E.D.Lazarus@soton.ac.uk](mailto:E.D.Lazarus@soton.ac.uk)

10 **ORCID**s

11 Lazarus 0000-0003-2404-9661

12 Harley 0000-0002-1329-7945

13 Blenkinsopp 0000-0001-5784-2805

14 Turner 0000-0001-9884-6917

15

16

17 **Abstract**

18 How storm events contribute to long-term shoreline change over decades to centuries  
19 remains an open question in coastal research. Sand and gravel coasts exhibit remarkable  
20 resilience to event-driven disturbances, and, in settings where sea level is rising, shorelines  
21 retain almost no detailed information about their own past positions. Here, we use a  
22 detailed, multi-decadal observational record of shoreline position to demonstrate  
23 quantitative indications of morphodynamic turbulence – "signal shredding" – in a sandy  
24 beach system. We find that, much like other dynamic sedimentary systems, processes of  
25 sediment transport that affect shoreline position at relatively short time-scales obscure or  
26 erase physical evidence of external forcing. This suggests that large forcing events like  
27 major coastal storms, even when their effects are recorded, may convey less about the  
28 dynamics of long-term shoreline change – and vice versa – than coastal researchers might  
29 wish.

30

31 **Keywords** – coastal hazard; landscape resilience; beach recovery; beach rotation;  
32 Narrabeen-Collaroy



## 33 1. Introduction

34 Quantifying magnitudes and rates of shoreline change is fundamental to understanding the  
35 dynamics of coastlines: not only how they behave over time, but also how they may  
36 respond to future, climate-related changes in environmental forcing. From a coastal-  
37 management perspective, shoreline change may constitute a coastal hazard – either event-  
38 driven, like the impact of a major storm, or chronic, like persistent shoreline erosion from a  
39 net-negative sediment budget. Long-term, continuous measurement of shoreline position  
40 observed at a given location will record changes arising from event-driven and chronic  
41 forcing, alike. But how punctuated storm events contribute to long-term shoreline change  
42 (over decades to centuries) remains an open question, particularly in the context of  
43 shoreline-change prediction (Morton et al., 1994; Fenster et al., 2001; Houser and  
44 Hamilton, 2009; Anderson et al., 2010; Masselink and van Heteren, 2014; Brooks et al.,  
45 2016; Masselink et al., 2016; Scott et al., 2016; Burvingt et al., 2017).

46 Evidence of coastal storm frequency and magnitude over centuries to millennia may be  
47 stored in the sedimentary stratigraphy of beach ridges (Tamura, 2012) and washover into  
48 back-barrier lagoons (Donnelly and Woodruff, 2007), offering a window into climatic  
49 conditions in the recent geologic past. But ridge or washover stratigraphy is not a direct  
50 measure of shoreline position. Indeed, in transgressive settings (in which relative sea level is  
51 rising) the shoreline itself retains almost no detailed information about its own past  
52 positions. Sand and gravel coastlines, especially, reflect remarkable resilience to event-  
53 driven disturbances – even to tsunamis (Choowong et al., 2009). Storm-driven shoreline  
54 excursions on the order of  $\sim 10^1$ – $10^2$  m may be obscured in the shoreline position (and/or  
55 beach volume) within days to months, and effectively erased within years (Birkemeir, 1979;  
56 Egense, 1989; Thom and Hall, 1991; Morton et al., 1994; Douglas and Crowell, 2000;  
57 Honeycutt et al., 2001; Zhang et al., 2002; List et al., 2006; Lazarus et al., 2012; Lentz et al.,  
58 2013; Masselink and van Heteren, 2014; Phillips et al., 2017).

59 This context echoes a theoretical exposition by Jerolmack and Paola (2010) regarding the  
60 problem of determining how dynamic sedimentary systems – especially those with source-  
61 to-sink pathways – respond to rapid external forcing. Processes of sediment transport tend  
62 to rework upstream/upslope inputs so completely that their downstream/downslope  
63 outputs may bear no resemblance to the original pattern of forcing that drove them.  
64 Jerolmack and Paola (2010) call this phenomenon the "shredding" of environmental  
65 signals, and offer that shredding – or, more formally, "morphodynamic turbulence" –  
66 behaves much like fluid turbulence, in that "energy injected at one frequency is smeared  
67 across a range of scales." High-frequency signals of external forcing are especially likely to  
68 be shredded. Drawing on the physics of turbulent fluid flows (Frisch and Kolmogorov,  
69 1995), Jerolmack and Paola (2010) use sediment flux time-series from physical and  
70 numerical experiments – bedload transport in a flume channel (Singh et al., 2009), a  
71 canonical rice-pile experiment (Frette et al., 1996), and a numerical rice-pile model – to  
72 illustrate their argument. Beyond source-to-sink sedimentary systems (Romans et al., 2016),  
73 signal shredding has since been extended to spatio-temporal changes in lake levels  
74 (Williams and Pelletier, 2015) and methane release from peatlands (Ramirez et al., 2015).



75 Here, we investigate signal shredding in an altogether different sediment-transport system:  
76 that of a sandy beach. Although previous studies of sandy shoreline dynamics have invoked  
77 signal shredding conceptually (Lazarus et al., 2011, 2012; Williams et al., 2013), none have  
78 used observed shoreline data to demonstrate quantitative signatures of signal shredding  
79 empirically. Following Jerolmack and Paola (2010), we find the hallmarks of  
80 morphodynamic turbulence in observational time series of shoreline position at Narrabeen-  
81 Collaroy Beach, southeast Australia (Short and Trembanis, 2004; Harley et al. 2011, 2015;  
82 Turner et al. 2016; Phillips et al., 2017). The potential for beaches to "shred" large-  
83 magnitude changes in shoreline position complicates reconciliation of short-term beach  
84 dynamics and long-term, spatio-temporal patterns of shoreline variability and evolution.

## 85 2. Setting and dataset

86 The Narrabeen-Collaroy embayment (Fig. 1a) comprises a 3.6 km long sandy beach, and is  
87 one of only a few sites worldwide where ongoing beach monitoring has been regular,  
88 frequent, and uninterrupted for multiple decades (Turner et al., 2016). Cross-shore profiles  
89 at five locations along the beach (Fig. 1a) have been measured approximately monthly (Fig.  
90 1b) since 1976 (Turner et al., 2016). In addition to more than four decades of these  
91 monthly cross-shore beach profiles, continuous alongshore shoreline positions derived  
92 from RTK-GPS quadbike surveys of the full three-dimensional subaerial beach have been  
93 obtained approximately monthly (Fig. 1c) since 2005 (Harley and Turner 2008; Harley et  
94 al., 2011, 2015). For the southern half of the embayment (Fig. 1a), daily-averaged shoreline  
95 position has also been recorded by an Argus Coastal Imaging system (Fig. 1d) for over a  
96 decade (Phillips et al., 2017). In each of these sets we take the 0.7 m AHD (Australian  
97 Height Datum) elevation contour as the shoreline, commensurate with mean high water  
98 (Harley et al., 2011). Data gaps in the profiles and time-series are filled by linear  
99 interpolation.

## 100 3. Analysis

### 101 3.1. Patterns in power spectra

102 In their bedload and rice-pile examples, Jerolmack and Paola (2010) collapse these physical  
103 systems into one dimension – a time series of sediment flux past a single point – defining  
104 sediment flux ( $q$ ) as the instantaneous quantity of sediment leaving the system. Here, in our  
105 beach example, we define  $q$  as the change in shoreline position ( $x$ , where elevation  $z = 0.7$   
106 m AHD) between consecutive time steps at a given location alongshore ( $y$ ) (Fig. 2a–f). In a  
107 generic source-to-sink system in which sediment only moves downstream, sediment flux is  
108 unidirectional and positive. By contrast, in the one-dimensional beach system explored  
109 here, shoreline movement is bidirectional, as wave-driven cross-shore sediment transport  
110 shifts the shoreline at any location ( $x, y$ ) onshore and offshore over time. We therefore use  
111 both the positive and negative values of shoreline change to represent sediment flux.

112 Like the systems described by Jerolmack and Paola (2010), a power spectrum of the one-  
113 dimensional sediment-flux term  $q(t)$  yields a pattern with two regimes. A non-stationary  
114 regime, in which spectral density increases as a power-law function of time-scale over  
115 shorter intervals, transitions or rolls over into a comparatively stationary (or uncorrelated)



116 regime at longer intervals (Fig. 2g–i). Although less crisply defined than the modeled  
117 unidirectional examples from Jerolmack and Paola (2010), this general pattern in the power  
118 spectrum serves as the first indication that signal shredding is inherent in the dynamics of  
119 sandy beach systems.

120 But what signal, exactly, is being shredded at the shoreline? Consider again a unidirectional  
121 source-to-sink system, driven by some input flux ( $q_o$ ) at the upstream end. That input flux  
122 might be constant; it might fluctuate (e.g., seasonal cycles); it might spike with large-  
123 magnitude events. Whatever its pattern in time, input flux embodies the environmental  
124 signal that is susceptible to shredding by sediment transport processes as it passes  
125 downstream through the system. In a controlled physical experiment or a numerical model,  
126 input flux (of sediment and/or fluid) is a known quantity, set by the researcher. For natural  
127 source-to-sink systems, sediment input flux cannot necessarily be resolved directly – but it  
128 may be estimated from flow discharge (i.e., bedload sediment flux will be a fraction of the  
129 fluid flux). Here, in the beach system, we assume that the input flux – the external  
130 environmental signal that shoreline behavior may destroy or preserve – is represented by  
131 energy flux from incident storm waves. We define storm wave conditions by a threshold  
132 corresponding to the 95th percentile of deep-water significant wave height ( $H_s$ , m), which  
133 for this region is  $H_s > 3$  m (Harley, 2017). Much like flow discharge in a fluvial system,  
134 deep-water wave energy flux ( $E$ , kW per m wavefront) may serve as a useful proxy for  
135 input flux to the beach:

$$136 \quad E = \frac{\rho g^2}{64\pi} H_s^2 P_w \approx 0.5 H_s^2 P_w \text{ kW/m} \quad (1)$$

137 where  $\rho$  ( $\text{kg/m}^3$ ) is water density,  $g$  ( $\text{m/s}^2$ ) is acceleration by gravity,  $H_s$  (m) is significant  
138 deep-water wave height, and  $P_w$  (s) is wave period.

139 We calculate monthly and daily total storm-wave energy flux corresponding to the monthly  
140 and daily shoreline time-series (Fig. 3a,b), and transform them into power spectra (Fig.  
141 3c,d). The consistent spectral pattern encoded in the time-series of shoreline change ( $q$ )  
142 appears to be more organized (Fig. 2g–i) than the one encoded in the wave forcing ( $q_o$ )  
143 (Fig. 3c,d). Where the power spectrum for  $q$  is non-stationary over a range of relatively  
144 high frequencies (short time-scales relative to the total length of the time-series) before  
145 transitioning into a comparatively stationary regime, the power spectrum for  $q_o$  is  
146 effectively stationary across all time-scales.

147 According to Jerolmack and Paola (2010), the transition in spectral density from non-  
148 stationary to stationary should correspond to an intrinsic, characteristic time-scale  $T_x$ .  
149 Theoretically,  $T_x$  is set by the system size  $L$  and sediment input rate  $q_o$ . While those  
150 parameters can be dictated for experimental systems and calculated reasonably for  
151 (unidirectional) source-to-sink systems, they are less clear for an open sandy coastline. We  
152 estimate  $T_x$  in the Narrabeen-Collaroy system through two independent approaches.

### 153 3.1 Characteristic time-scale from system size and input flux

154 The first approach is a back-of-the-envelope exercise. We assume that the system size  $L$  is  
155 equivalent to maximum cross-shore beach width. This assumption follows from having



156 collapsed the system into only the cross-shore ( $x$ ) dimension: for any alongshore position  $y$ ,  
157 the theoretical maximum cross-shore ( $x$ ) extent to which the beach can ever erode is the  
158 full width of the beach  $L$ , independent of embayment length. (We call  $L$  the "theoretical  
159 maximum" because historical records of shoreline change are necessarily of finite duration,  
160 and therefore may never reflect this full width.) Since  $q$  and  $E$  have different units, for this  
161 calculation we normalize both time-series relative to their respective maximum values.  
162 Thus, at all profiles  $L = 1$ . For  $q_o$ , we take the mean normalized monthly (and daily) total  
163 wave energy flux over the full span of the dataset. This representation of mean  $q_o$  is an  
164 imperfect proxy for the kind of constant input flux possible with a sediment feeder in  
165 controlled experiments, but it serves the purpose here for a rough estimate of  $T_x$ . Dividing  
166  $L/q_o$  for the monthly total time-series (Fig. 3a) yields  $T_x = \sim 180$  days ( $\sim 6$  months), and for  
167 the daily total time-series (Fig. 3b) yields  $T_x = \sim 150$  days ( $\sim 5$  months).

### 168 3.2 Characteristic time-scale from modes of beach dynamics

169 The second approach to estimate one or more characteristic time-scales  $T_x$  for the  
170 Narrabeen-Collaroy system is based on observed modes of shoreline behavior typical at  
171 this site, and at embayed beaches more generally (Ranasinghe et al, 2004; Harley et al.,  
172 2011, 2015; Ratliff and Murray, 2014). Although modes vary in detail between specific  
173 locations, approximately four modes of shoreline behavior tend to describe how sediment  
174 moves within embayed beach systems. One mode reflects cycles of off- and onshore  
175 movement of sediment as a quasi-coherent unit at the full scale of the embayment (i.e.,  
176 imagine a narrow beach during stormier times of the year, and a wide beach during calmer  
177 intervals). Another dominant mode of shoreline response is termed "rotation," and occurs  
178 when prevailing wave conditions or a storm event shifts a significant volume of sediment  
179 inside the embayment alongshore and/or onshore-offshore to form a wider beach at one  
180 end and a narrower beach at the other (Ranasinghe et al, 2004). Related to this rotation is  
181 what has been described as a "breathing" mode, a kind of shoreline resonance that hinges  
182 near the center of the beach and characterizes changes in shoreline curvature, as sand  
183 moves between the middle and ends of an embayment (Ratliff and Murray, 2014). Another  
184 potential mode of shoreline dynamics reflects patterns of shoreline variability introduced  
185 by rhythmic movements of sandbars, sandwaves, megacusps, and inlet processes, where  
186 applicable (Harley et al., 2011, 2015). These four modes are not necessarily hierarchical:  
187 their relative dominance can change as a function of wave conditions. More importantly,  
188 these principle modes of shoreline behavior likely manifest intrinsic time-scales.

189 To find characteristic time-scales corresponding to the modes of shoreline behavior at  
190 Narrabeen-Collaroy, we follow steps described by Ratliff and Murray (2014). From the  
191 monthly shorelines derived from RTK-GPS quadbike surveys, at each position alongshore  
192 we detrend the series of shoreline position (not shoreline-position change) in time (Fig. 4a).  
193 To calculate the empirical orthogonal modes in the alongshore dimension through time,  
194 and thus characterize shoreline variation around its mean position (Fig. 4b), we apply  
195 principal-component analysis. Each mode in sequence explains a smaller percentage of  
196 variation in the data. We then use a continuous wavelet transform to examine the spectral  
197 signatures of the first four modes in the temporal dimension, squaring the wavelet



198 transform coefficients and finding the mean power at each wavelet scale for time. The  
199 result is a power spectrum (Lazarus et al., 2011), in which peaks represent the characteristic  
200 time-scale for each mode of embayed-beach behavior (Ratliff and Murray, 2014). We take  
201  $T_x$  (Fig. 4c) as the first local maximum in the power spectrum (Ratliff and Murray, 2014)  
202 using a Ricker-Marr wavelet. (Other Gaussian-type wavelets yield similar power spectra and  
203 characteristic time-scales.)

204 We find that the first two modes in these data are both rotational (Fig. 4c): the first, a  
205 rotation toward the north, accounts for 51% of the observed shoreline variability with a  
206 characteristic time-scale of  $\sim 21$  months; the second, a rotation toward the south, accounts  
207 for 32% ( $\sim 6.5$  months), and agrees closely with the  $T_x$  calculated independently from the  
208 (normalized) cumulative wave-energy flux data. The third and fourth modes account for  
209 5.4% ( $\sim 11$  months) and 2.5% ( $\sim 11$  months) of observed shoreline variability, respectively.  
210 In previous applications of PCA to Narrabeen-Collaroy (Short and Trembanis, 2004;  
211 Harley et al., 2011, 2015), rotational behavior was secondary (26% of shoreline variability  
212 around its mean position) to a dominant mode ( $\sim 60\%$ ) of quasi-coherent, off- and onshore  
213 sand movement within the embayment.

#### 214 4. Discussion and implications

215 Jerolmack and Paola (2010) show that morphodynamic turbulence will tend to "shred"  
216 (strongly modify) input perturbations with time-scales shorter than the characteristic time-  
217 scale of the system ( $T < T_x$ ). Only input perturbations with time-scales  $T > T_x$  are likely to  
218 be preserved (or only weakly modified) in the output flux  $q$ . The characteristic time-scales  
219 that we estimate for the Narrabeen-Collaroy system (Figs. 3 and 4) suggest that shoreline-  
220 change perturbations with time-scales  $T < T_x$  (where  $T_x \approx 6$  months) fall within the bounds  
221 of morphodynamic turbulence, and their effects on shoreline change will tend to get  
222 "smeared" across a range of temporal scales in the output signal (Fig. 2). In these data, a  
223 seasonal time-scale ( $\sim 6$  months) appears to dominate (Fig. 2g–i). Irregular but multi-annual  
224 forcings, such as the El Niño–Southern Oscillation (Barnard et al., 2015), should therefore  
225 have a time-scale sufficiently long enough to avoid erasure by seasonal cycling. Moreover,  
226 if climate-related drivers were to increase future forcing at the seasonal time-scale ( $T \approx T_x$ ),  
227 there is potential for system resonance (Binder et al., 1995; Cadot et al., 2003; Jerolmack  
228 and Paola, 2010) to amplify seasonal shoreline changes.

229 Only an exceptional event, Jerolmack and Paola (2010) argue, whatever its time-scale, may  
230 be large enough to travel through a unidirectional sediment-transport system without being  
231 shredded. They point out that in morphodynamic systems defined by critical thresholds  
232 (landsliding in an experimental rice pile, for example), a minor perturbation can cascade  
233 from small scales to large ones, amplifying into a "system-clearing event." They conclude  
234 that although morphodynamic turbulence and fluid turbulence share similar scaling, the  
235 tendency to cascade implies that morphodynamic turbulence, contrary to its fluid  
236 counterpart, is not dissipative. We suggest that sandy coastlines may exemplify a  
237 sedimentary system in which morphodynamic turbulence is dissipative. Unlike threshold-  
238 driven systems of unidirectional flow where amplification is possible, the maximum



239 magnitude of a system-clearing event in an embayed beach cannot exceed the theoretical  
240 maximum beach width  $L$ . Forcing by wave-energy flux might vary over time (Harley et al.,  
241 2011, 2015; Ratliff and Murray, 2014; Phillips et al., 2017), but alongshore sediment  
242 transport resulting from prevailing waves will tend to smooth out plan-view perturbations  
243 in shoreline position on a sandy coast, at least over relatively local spatial scales ( $< \sim 10^3$  m)  
244 and where shoreline curvature is low (Lazarus and Murray, 2007; Lazarus et al., 2011,  
245 2012).

246 The predominance of dissipative effects and a characteristic  $T_x$  at the seasonal time-scale  
247 and will tend to make storm-driven perturbations in shoreline-position time-series difficult  
248 to isolate in sparsely sampled records of shoreline change. If cross-shore beach recovery is  
249 rapid – that is, if most of the sediment shifted off a beach during a storm is stored in a  
250 nearshore bar and then swept back onshore in a matter of days to weeks afterward – then  
251 the magnitude of shoreline change driven by the event may appear damped in even a  
252 monthly survey of beach position. In cases where alongshore sediment transport is  
253 significant, then the longer the beach, the more effective the shredder. When such large  
254 fluctuations are so ephemeral, only high-frequency sampling can hope to capture their  
255 fullest extents (Splinter et al., 2013; Phillips et al., 2017).

256 Intrinsic time-scales for modes of beach change along open coastlines may be different  
257 from those for embayed settings. Ratliff and Murray (2014) suggest the diffusive scaling  
258 evident in their modeling results implies that characteristic time-scales increase nonlinearly  
259 with embayment length alongshore. They list other factors that could likewise change the  
260 characteristic time-scales, such as wave height, sediment type, and the aspect ratio of  
261 headlands relative to the bay (which would affect local wave height through wave  
262 shadowing). Were the same high-resolution spatio-temporal data available for  $\sim 10^4$  m of  
263 open sandy coastline as it is for Narrabeen-Collaroy, comparable analysis might highlight a  
264 series of progressively larger characteristic time-scales for reversing erosion hotspots,  
265 alongshore sand waves, and fluctuations in alongshore curvature (List et al., 2006; Lazarus  
266 et al., 2011).

267 In an ideal source-to-sink sedimentary system with perfect storage, output flux  $q$  would be  
268 faithfully recorded in the sink stratigraphy. The majority of work in morphodynamic  
269 turbulence and signal shredding comes from efforts to puzzle out what information  
270 stratigraphic records do and do not convey about environmental forcing (Paola et al.,  
271 2018). Since shoreline position in a transgressive beach system is not stored in any way  
272 comparable to a source-to-sink system, what does it mean to represent shoreline change as  
273 sedimentary output flux? The answer may be that large forcing events like major coastal  
274 storms, even when we can record their effects, probably tell us less about the dynamics of  
275 long-term shoreline change – and vice versa – than we wish to know. In embayed beach  
276 systems where alongshore spatial scales are constrained ( $< \sim 10^1$  km), cross-shore sediment  
277 cycling and rotational 'sloshing' of the beach between headlands combine to make a highly  
278 efficient shredder that operates at the full spatial extent of the beach. On open coastlines,  
279 where alongshore spatial scales are large ( $\sim 10^1$ – $10^2$  km), the cumulative, diffusive effect of  
280 alongshore sediment transport is an equally effective shredder (Lazarus et al., 2011, 2012) –



281 and likely even more so when coupled to human manipulations of natural shoreline  
282 behavior (McNamara and Werner, 2008a,b; Williams et al., 2013; Lazarus et al., 2011;  
283 Lazarus et al., 2016).

284 Empirical evidence of signal shredding in the shoreline-position data from the Narrabeen-  
285 Collaroy system demonstrates how, and suggests why, signatures of individual storm  
286 impacts can be obscured or erased in long-term observational records, even those recorded  
287 at a reasonably high (~monthly) temporal resolution. Jerolmack and Paola (2010)  
288 recommend using controlled experiments to gain vital mechanistic insight into  
289 morphodynamic turbulence. Here, the effects of system size  $L$ , input flux  $q_0$ , the  
290 magnitudes of so-called "system-clearing events," and potential resonant amplification ( $T \approx$   
291  $T_c$ ) at seasonal time-scales could be tested systematically across a broad parameter space for  
292 coastal systems. In exploring the dynamics of signal shredding, the same controlled  
293 experiments that would also be exploring characteristic time-scales for fundamental  
294 processes of sediment transport in coastal environments.

295

#### 296 **Acknowledgements**

297 EDL thanks A. Ashton and D. McNamara for discussions, dating back to the publication  
298 of Jerolmack and Paola (2010), about signal shredding in shoreline data. This work was  
299 supported by funding (to EDL) from the NERC BLUEcoast project (NE/N015665/2)  
300 and a University of Southampton Global Partnerships Award. Since 2004, the ongoing  
301 beach monitoring program at Narrabeen-Collaroy has been funded by the Australian  
302 Research Council (Discovery and Linkage), Warringah and Northern Beaches Councils,  
303 NSW Office of Environment and Heritage (OEH), SIMS foundation, and the UNSW  
304 Faculty of Engineering (see Turner et al., 2016).

305

306

#### 307 **References**

- 308 Anderson, T. R., Frazer L. N., and Fletcher C. H.: Transient and persistent shoreline  
309 change from a storm, *Geophys. Res. Lett.*, 37, L08401, doi:[10.1029/2009GL042252](https://doi.org/10.1029/2009GL042252), 2010.
- 310 Ashton, A., Murray, A. B., and Arnault, O.: Formation of coastline features by large-scale  
311 instabilities induced by high-angle waves, *Nature*, 414(6861), 296–300, 2001.
- 312 Ashton, A. D., and Murray, A. B.: High-angle wave instability and emergent shoreline  
313 shapes: 1. Modeling of sand waves, flying spits, and capes, *J. Geophys. Res. Earth*, 111(F4),  
314 doi:[10.1029/2005JF000422](https://doi.org/10.1029/2005JF000422), 2006a.
- 315 Ashton, A. D., and Murray, A. B.: High-angle wave instability and emergent shoreline  
316 shapes: 2. Wave climate analysis and comparisons to nature, *J. Geophys. Res. Earth*,  
317 111(F4), doi: [10.1029/2005JF000423](https://doi.org/10.1029/2005JF000423), 2006b.
- 318 Barnard, P. L., Short, A. D., Harley, M. D., Splinter, K. D., Vitousek, S., Turner, I. L.,  
319 Allen, J., Banno, M., et al.: Coastal vulnerability across the Pacific dominated by El  
320 Niño/Southern Oscillation, *Nat. Geosci.*, 8(10), 801–807, 2015.



- 321 Binder, G., Tardu, S., and Vezin, P.: Cyclic modulation of Reynolds stresses and length  
322 scales in pulsed turbulent channel flow, *Proc. R. Soc. Lond. A*, 451(1941), 121–139, 1995.
- 323 Birkemeier, W. A.: The effects of the 19 December 1977 coastal storm on beaches in  
324 North Carolina and New Jersey, USACE Coastal Engineering Research Center, 1979.
- 325 Brooks, S. M., Spencer, T., McIvor, A., and Möller, I.: Reconstructing and understanding  
326 the impacts of storms and surges, southern North Sea, *Earth Surf. Proc. Land.*, 41(6), 855–  
327 864, 2016.
- 328 Burvingt, O., Masselink, G., Russell, P., and Scott, T.: Classification of beach response to  
329 extreme storms, *Geomorphology*, 295, 722–737, 2017.
- 330 Cadot, O., Titon, J. H., and Bonn, D.: Experimental observation of resonances in  
331 modulated turbulence, *J. Fluid Mech.*, 485, 161–170, 2003.
- 332 Choowong, M., Phantuwoongraj, S., Charoentitirat, T., Chutakositkanon, V., Yumuang, S.,  
333 and Charusiri, P.: Beach recovery after 2004 Indian Ocean tsunami from Phang-nga,  
334 Thailand, *Geomorphology*, 104(3), 134–142, 2009.
- 335 Donnelly, J. P., and Woodruff, J. D.: Intense hurricane activity over the past 5,000 years  
336 controlled by El Niño and the West African monsoon, *Nature*, 447(7143), 465–468, 2007.
- 337 Douglas, B. C., and Crowell, M.: Long-term shoreline position prediction and error  
338 propagation, *J. Coastal Res.*, 16(1), 145–152, 2000.
- 339 Egense, A. K.: Southern California beach changes in response to extraordinary storm,  
340 *Shore and Beach*, 57(4), 14–17, 1989.
- 341 Fenster, M. S., Dolan, R., and Morton, R. A.: Coastal storms and shoreline change: signal  
342 or noise? *J. Coastal Res.*, 17(3), 714–720, 2001.
- 343 Frette, V., Christensen, K., Malthe-Sorensen, A., and Feder, J.: Avalanche dynamics in a  
344 pile of rice, *Nature*, 379(6560), 49–52, 1996.
- 345 Frisch, U., and Kolmogorov, A. N.: *Turbulence: The legacy of A.N. Kolmogorov*,  
346 Cambridge Univ. Press, Cambridge, 1995.
- 347 Harley, M. D.: Coastal storm definition, in: Ciavola, P., Coco, G. (Eds.), *Coastal Storms:*  
348 *Processes and Impacts*, John Wiley and Sons, 1–21, 2017.
- 349 Harley, M. D., and Turner, I. L.: A simple data transformation technique for pre-  
350 processing survey data at embayed beaches, *Coastal Eng.*, 55(1), 63–68, 2008.
- 351 Harley, M. D., Turner, I. L., Short, A. D., and Ranasinghe, R.: A reevaluation of coastal  
352 embayment rotation: The dominance of cross-shore versus alongshore sediment transport  
353 processes, Collaroy-Narrabeen Beach, southeast Australia, *J. Geophys. Res. Earth*, 116(F4),  
354 doi:[10.1029/2011JF001989](https://doi.org/10.1029/2011JF001989), 2011.
- 355 Harley, M. D., Turner, I. L., and Short, A. D.: New insights into embayed beach rotation:  
356 The importance of wave exposure and cross-shore processes, *J. Geophys. Res. Earth*,  
357 120(8), 1470–1484, 2015.
- 358 Honeycutt, M. G., Crowell, M., and Douglas, B. C.: Shoreline-position forecasting: impact  
359 of storms, rate-calculation methodologies, and temporal scales, *J. Coastal Res.*, 17(3), 721–  
360 730, 2001.
- 361 Jerolmack, D. J., and Paola, C.: (2010). Shredding of environmental signals by sediment  
362 transport, *Geophys. Res. Lett.*, 37(19), doi:[10.1029/2010GL044638](https://doi.org/10.1029/2010GL044638), 2010.



- 363 Lazarus, E. D., and Murray, A. B.: Process signatures in regional patterns of shoreline  
364 change on annual to decadal time scales, *Geophys. Res. Lett.*, 34(19),  
365 doi:[10.1029/2007GL031047](https://doi.org/10.1029/2007GL031047), 2007.
- 366 Lazarus, E., Ashton, A., Murray, A. B., Tebbens, S., and Burroughs, S.: Cumulative versus  
367 transient shoreline change: Dependencies on temporal and spatial scale, *J. Geophys. Res.*  
368 *Earth*, 116(F2), doi:[10.1029/2010JF001835](https://doi.org/10.1029/2010JF001835), 2011.
- 369 Lazarus, E. D., Mcnamara, D. E., Smith, M. D., Gopalakrishnan, S., and Murray, A. B.:  
370 Emergent behavior in a coupled economic and coastline model for beach nourishment,  
371 *Nonlinear Proc. Geoph.*, 18, 989–999, 2011.
- 372 Lazarus, E. D., Ashton, A. D., and Murray, A. B.: Large-scale patterns in hurricane-driven  
373 shoreline change, in *Extreme events and natural hazards: the complexity perspective*,  
374 Sharma, A. S., Bunde, A., Dimri, V. P. and Baker, D. N. (Eds.), AGU Geophysical  
375 Monograph Series, 196, 127–138, 2012.
- 376 Lazarus, E. D., Ellis, M. A., Murray, A. B., and Hall, D. M.: An evolving research agenda  
377 for human–coastal systems, *Geomorphology*, 256, 81–90, 2016.
- 378 Lentz, E. E., Hapke, C. J., Stockdon, H. F., and Hehre, R. E.: Improving understanding of  
379 near-term barrier island evolution through multi-decadal assessment of morphologic  
380 change, *Mar. Geol.*, 337, 125–139, 2013.
- 381 List, J. H., Farris, A. S., and Sullivan, C.: (2006). Reversing storm hotspots on sandy  
382 beaches: spatial and temporal characteristics, *Mar. Geol.*, 226, 261–279, 2006.
- 383 Masselink, G., and van Heteren, S.: Response of wave-dominated and mixed-energy  
384 barriers to storms. *Mar. Geol.*, 352, 321–347, 2014.
- 385 Masselink, G., Castelle, B., Scott, T., Dodet, G., Suanez, S., Jackson, D., and Floe'h, F.:  
386 Extreme wave activity during 2013/2014 winter and morphological impacts along the  
387 Atlantic coast of Europe, *Geophys. Res. Lett.*, 43(5), 2135–2143.
- 388 Mcnamara, D. E., and Werner, B. T.: Coupled barrier island–resort model: 1. Emergent  
389 instabilities induced by strong human-landscape interactions, *J. Geophys. Res. Earth*,  
390 113(F1), doi:[10.1029/2007JF000840](https://doi.org/10.1029/2007JF000840), 2008a.
- 391 Mcnamara, D. E., and Werner, B. T.: Coupled barrier island–resort model: 2. Tests and  
392 predictions along Ocean City and Assateague Island National Seashore, Maryland, *J.*  
393 *Geophys. Res. Earth*, 113(F1), doi:[10.1029/2007JF000841](https://doi.org/10.1029/2007JF000841), 2008b.
- 394 Morton, R. A., Paine, J. G., and Gibeaut, J. C.: Stages and durations of post-storm beach  
395 recovery, southeastern Texas coast, USA, *J. Coastal Res.*, 10(4), 884–908, 1994.
- 396 Paola, C., Ganti, V., Mohrig, D., Runkel, A. C., and Straub, K. M.: Time not our time:  
397 Physical controls on the preservation and measurement of geologic time, *Annu. Rev. Earth*  
398 *Pl. Sci.*, 46, 409–438, 2018.
- 399 Phillips, M. S., Harley, M. D., Turner, I. L., Splinter, K. D., and Cox, R. J.: Shoreline  
400 recovery on wave-dominated sandy coastlines: the role of sandbar morphodynamics and  
401 nearshore wave parameters, *Mar. Geol.*, 385, 146–159, 2017.
- 402 Ramirez, J. A., Baird, A. J., Coulthard, T. J., and Waddington, J. M.: Ebullition of methane  
403 from peatlands: Does peat act as a signal shredder? *Geophys. Res. Lett.*, 42(9), 3371–3379,  
404 2015.

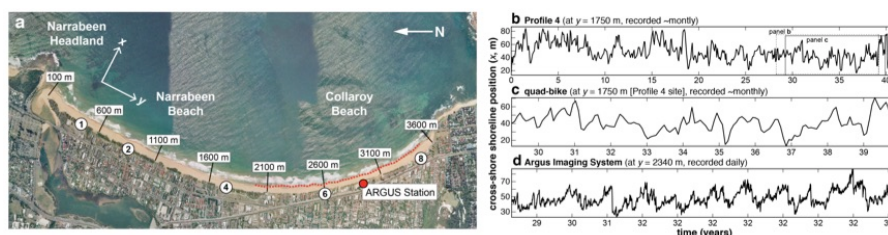


- 405 Ranasinghe, R., McLoughlin, R., Short, A., and Symonds, G.: The Southern Oscillation  
406 Index, wave climate, and beach rotation, *Mar. Geol.*, 204(3-4), 273–287, 2004.
- 407 Ratliff, K. M., and Murray, A. B.: Modes and emergent time scales of embayed beach  
408 dynamics, *Geophys. Res. Lett.*, 41(20), 7270–7275, 2014.
- 409 Romans, B. W., Castelltort, S., Covault, J. A., Fildani, A., and Walsh, J. P.: Environmental  
410 signal propagation in sedimentary systems across timescales, *Earth-Sci. Rev.*, 153, 7–29,  
411 2016.
- 412 Scott, T., Masselink, G., O'Hare, T., Saulter, A., Poate, T., Russell, P., Davidson, M. and  
413 Conley, D.: The extreme 2013/2014 winter storms: Beach recovery along the southwest  
414 coast of England, *Mar. Geol.*, 382, 224–241, 2016.
- 415 Short, A. D., and Trembanis, A. C.: Decadal scale patterns in beach oscillation and rotation  
416 Narrabeen Beach, Australia: time series, PCA and wavelet analysis, *J. Coastal Res.*, 523–  
417 532, 2004.
- 418 Singh, A., Fienberg, K., Jerolmack, D. J., Marr, J., and Foufoula-Georgiou, E.:  
419 Experimental evidence for statistical scaling and intermittency in sediment transport rates,  
420 *J. Geophys. Res. Earth*, 114(F1), doi:10.1029/2007JF000963, 2009.
- 421 Splinter, K. D., Turner, I. L., and Davidson, M. A.: How much data is enough? The  
422 importance of morphological sampling interval and duration for calibration of empirical  
423 shoreline models, *Coastal Eng.*, 77, 14–27, 2013.
- 424 Tamura, T.: Beach ridges and prograded beach deposits as palaeoenvironment records,  
425 *Earth-Sci. Rev.*, 114(3-4), 279–297, 2012.
- 426 Thom, B. G., and Hall, W.: Behaviour of beach profiles during accretion and erosion  
427 dominated periods, *Earth Surf. Proc. Land.*, 16(2), 113–127, 1991.
- 428 Turner, I. L., Harley, M. D., Short, A. D., Simmons, J. A., Bracs, M. A., Phillips, M. S., and  
429 Splinter, K. D.: A multi-decade dataset of monthly beach profile surveys and inshore wave  
430 forcing at Narrabeen, Australia, *Scientific Data*, 3, doi:10.1038/sdata.2016.24, 2016.
- 431 Williams, Z. C., and Pelletier, J. D.: Self-affinity and surface-area-dependent fluctuations of  
432 lake-level time series, *Water Resour. Res.*, 51(9), 7258–7269, 2015.
- 433 Williams, Z. C., McNamara, D. E., Smith, M. D., Murray, A. B., and Gopalakrishnan, S.:  
434 Coupled economic-coastline modeling with suckers and free riders, *J. Geophys. Res. Earth*,  
435 118(2), 887–899, 2013.
- 436 Zhang, K., Douglas, B., and Leatherman, S.: Do storms cause long-term beach erosion  
437 along the US East Barrier Coast? *J. Geol.*, 110(4), 493–502, 2002.



438 **Figures and Captions**

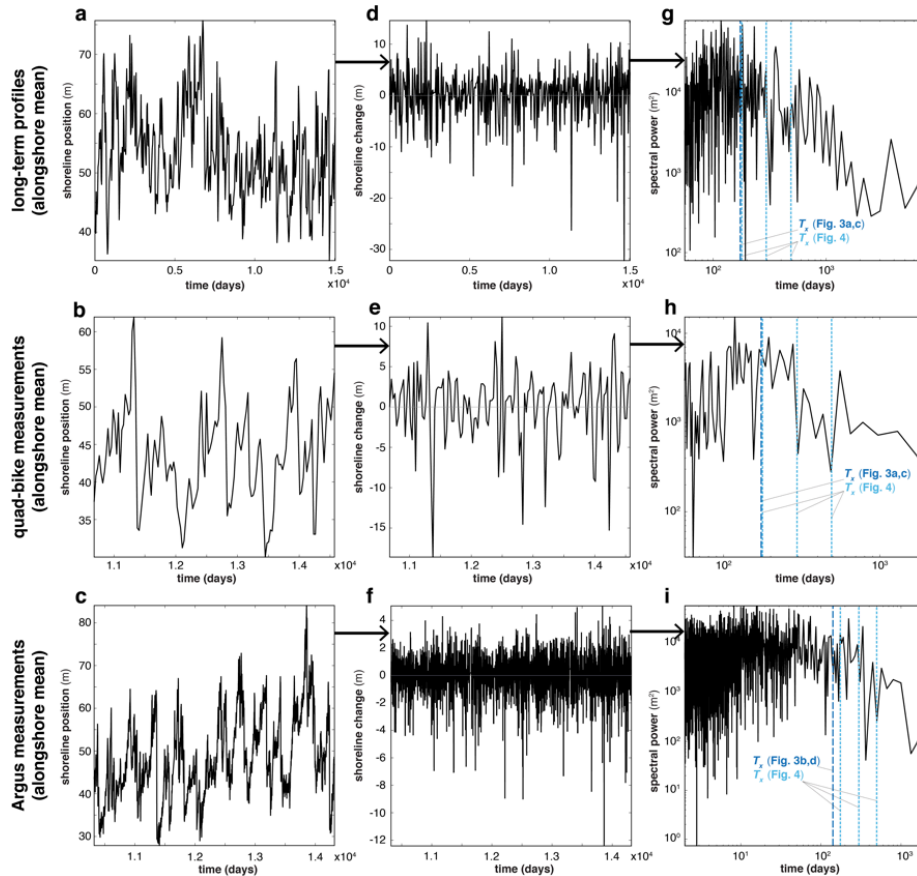
439



440

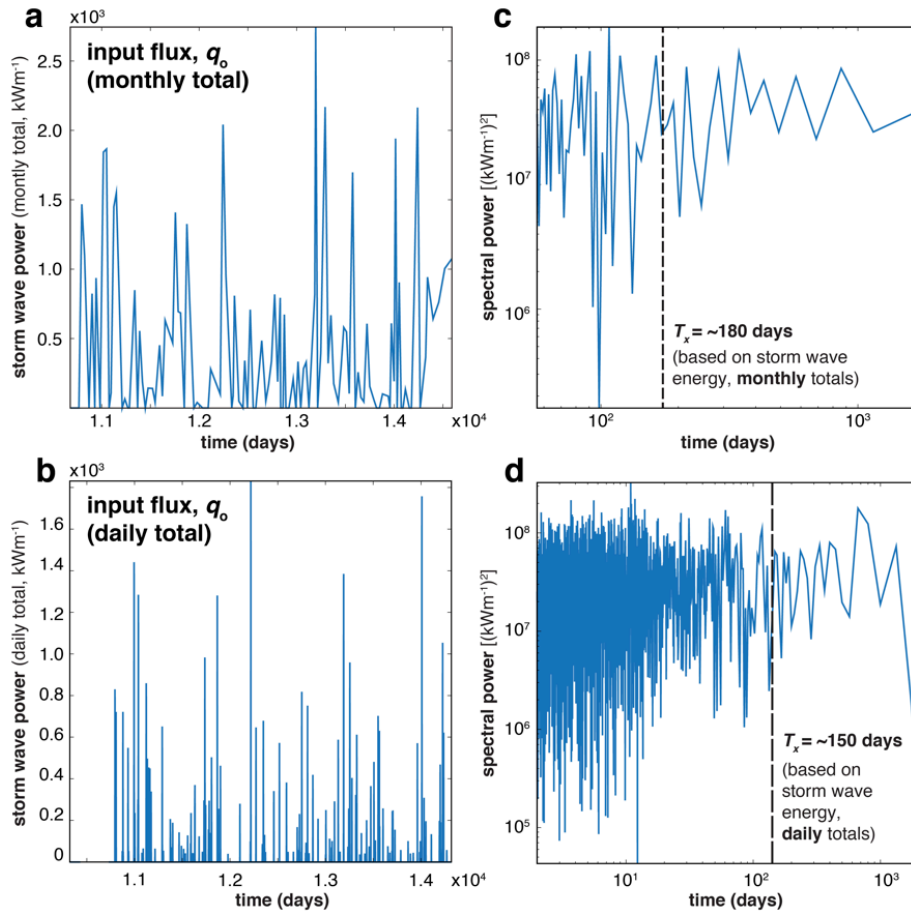
441 **Figure 1.** (a) Narrabeen-Collaroy beach, showing locations of long time-series profiles and  
442 Argus Imaging System coverage. Alongshore coordinates ( $y$ ) are relative to the northern  
443 end below Narrabeen Headland. (b) Long-term time series of cross-shore shoreline  
444 position (0.7 m contour) at Profile 4, measured approximately monthly between 1976–  
445 2017. Time axis is in years since first measurement (27 April 1976). (c) Time series of  
446 cross-shore shoreline position at alongshore location  $y = 1750$  m (aligned with Profile 4),  
447 measured by quad-bike approximately monthly between 2005–2017. (d) Time series of  
448 cross-shore shoreline position at alongshore location  $y = 2340$  m, measured by Argus  
449 Imaging System daily between 2005–2016. Boxes (dotted, solid) in panel (b) frame the  
450 temporal coverages for the time series in panels (c) and (d).

451



452

453 **Figure 2.** (a) Alongshore mean of monthly measurements of shoreline position ( $\bar{x} = 0.7$  m  
 454 contour) from long-term Profiles 1, 2, 4, 6, and 8, plotted in days since first measurement  
 455 (27 April 1976). (b) Alongshore mean of monthly shoreline position from the RTK-GPS  
 456 quad-bike surveys. (c) Alongshore mean shoreline position from a 850 m reach of the  
 457 Argus camera coverage ( $y = 1950\text{--}2800$  m). (d, e, f) Shoreline change in panels (a, b, c),  
 458 calculated as difference between consecutive shoreline positions, which we treat as output  
 459 flux  $q$ . (g, h, i) Resulting power spectra from panels (d, e, f), with estimated characteristic  
 460 time-scales  $T_x$  based on monthly/daily total storm wave energy flux (dashed line; Fig. 3),  
 461 and PCA of variations around mean shoreline position (dotted lines; Fig. 4).



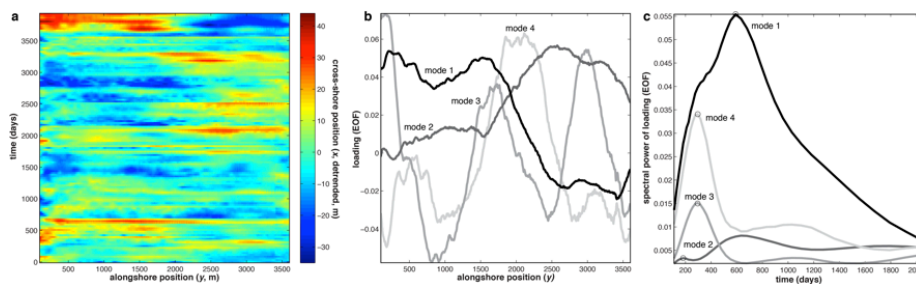
462

463 **Figure 3.** (a) Monthly total and (b) daily total storm wave energy flux between 2005–2017,  
 464 which we use as a proxy for input flux  $q_o$ . (c) Power spectrum for monthly total storm  
 465 wave energy flux in (a). Dotted line indicates estimated characteristic time-scale  $T_x = \sim 180$   
 466 days ( $\sim 6$  months). (d) Power spectrum for daily total storm wave energy flux in (b).  
 467 Dotted line indicates estimated characteristic time-scale  $T_x = \sim 150$  days ( $\sim 5$  months).

468



469



470

471 **Figure 4.** (a) Detrended (in time) shoreline position, measured ~monthly by quad-bike,  
472 with north at left (corresponding to Fig. 1a). (b) Orthogonal PCA modes, representing  
473 variance about the mean shoreline position, and (c) wavelet-derived power spectra (using a  
474 Ricker-Marr wavelet) of each mode, where the first local maximum indicates the  
475 characteristic time-scale ( $T_c$ ) for that mode.

476

477